Optimal clock speed of qubit gate operations on open quantum systems

Nilanjana Chanda [*] and Rangeet Bhattacharyya [†]
Department of Physical Sciences, Indian Institute of Science Education and Research Kolkata, Mohanpur 741246, West Bengal, India

(Received 8 August 2019; revised manuscript received 18 February 2020; accepted 16 March 2020; published 22 April 2020)

Efficient implementation of quantum algorithms requires single- or multiple-qubit gates with high fidelity. Here we report that the fidelity of gate operations on open quantum systems has a maximum value corresponding to an optimum value of the drive amplitude in the presence of drive-induced decoherence. To demonstrate this, we use a previously reported fluctuation-regulated quantum master equation [A. Chakrabarti and R. Bhattacharyya, Phys. Rev. A **97**, 063837 (2018)]. The fidelity is found to be a function of the drive-induced dissipative terms as well as the relaxation terms arising from the qubit-environment coupling; as a result, it behaves nonmonotonically with the drive amplitude. The existence of an optimum drive amplitude implies that the qubit gate operations on open quantum systems would have an optimal clock speed. We demonstrate the universality of the results for the gate operations on single- and multiple-qubit gates.

DOI: 10.1103/PhysRevA.101.042326

I. INTRODUCTION

Several quantum algorithms have been proved to be computationally superior to their classical counterparts [1–4]. Consequently, the physical realization of quantum computers has been a major area of research in the past couple of decades [5–12]. The conditions required for the physical realization of quantum computers were laid out by DiVincenzo [13], who argued that the operation time of quantum gates should be much smaller than the timescale of decoherence. Moreover, successful implementation of quantum algorithms requires not only the fulfillment of the DiVincenzo criteria, but also quantum gates of high fidelity to achieve reasonable fault tolerance. As a result, recent years have witnessed significant improvements in the implementation of high-fidelity gates on various architectures [10–12,14,15].

Among the recent works on high-fidelity gates, Ballance *et al.* implemented two-qubit and single-qubit logic gates using hyperfine trapped-ion qubits driven by Raman laser beams [14]. They experimentally found the maximum gate fidelity for a certain value of the gate time. The source of the variation in the value of the fidelity was attributed to the imperfection of the gate operations. In another recent work, Song *et al.* experimentally generated a ten-qubit entangled Greenberger-Horne-Zeilinger state using a superconducting circuit with the qubit-qubit interaction mediated by a bus resonator and created a ten-qubit quantum gate with a fidelity of 0.668 ± 0.025 [15]. Also, Huang *et al.* reported two-qubit randomized benchmarking with an average Clifford gate fidelity of 94.7% and an average controlled-rotation fidelity of 98% on silicon-based quantum dots [12].

These experiments were on systems of different physical origin and hence the varying fidelity could be due to either imperfect implementation of the gates because of instrumental imperfections or the dissipative nature of the systems due to coupling with the environment. While the former could be minimized in principle, the latter is much harder to remove, since no quantum system could be truly isolated. As such, one resorts to the standard description of driven-dissipative systems using the quantum master equation, which takes into account the relaxation terms originating from the environment to describe the nonunitary dynamics of the system. In the usual quantum master equations, the external drives on the system are included in the first order, whereas the system-environment coupling provides second-order nonunitary dissipators.

Recently, Chakrabarti and Bhattacharyya formulated a quantum master equation where an explicitly added environmental fluctuation provides a regulator in the dissipator terms [16]. This fluctuation-regulated quantum master equation (FRQME) has the Gorini-Kossakowski-Lindblad-Sudarshan (GKLS) form and hence is trace preserving and completely positive. The major advantage of such a formulation is that the external drives can also be included in the second order without requiring a rotating-wave approximation. The second-order contributions of the external drives have been shown to be of two types: (i) a shift term, which under an appropriate limit provides the dynamic Stark shift for detuned drives (and a Bloch-Siegert shift for a nonresonant component of the linearly polarized drive), and (ii) Kramers-Kronig pairs of the shift term which provides a pure dissipator which does not depend on the system-environment coupling strength. This dissipator originating from the drive has also been verified experimentally [17].

Previously, Bertaina *et al.* experimentally observed the decay of Rabi oscillations of spin qubits based on rare-earth ions and reported that the decay rate was found to depend

[*] nc16ip020@iiserkol.ac.in
[†] rangeet@iiserkol.ac.in

on the drive (microwave) power [18]. Similar drive-induced dissipation has earlier been observed experimentally in a variety of systems [19–22]. It has been shown how drive-induced dissipation can explain such behaviors reported in the above volume of works [16].

In the case of a resonant circularly polarized drive, the drive-induced dissipation (DID) survives, but the dynamic Stark shift term vanishes. As such, here we investigate the role of the DID in the realization of quantum gate operations. We show that the fast gate operations and achieving high fidelity may not be two independent processes in the presence of DID. We show that the competition between the two sources of decoherence, namely, system-environment coupling and second-order effects of the drive, naturally leads to an optimum value of the speed of single- or multiple-qubit gates. We will also introduce a simple measure of nonunitarity which helps quantify the performances of the gates.

II. DRIVEN-DISSIPATIVE DYNAMICS UNDER REGULARIZATION BY FLUCTUATIONS

Since the FRQME is relatively new in the history of quantum master equations, we present a brief sketch of its derivation. One begins with the premise that the thermal fluctuations take place in a thermal reservoir and could be explicitly represented by a suitably chosen Hamiltonian to complete the description of the local environment of a driven-dissipative system. As such, the general form of the Hamiltonian for the system and the local environment in the frequency unit may be written as

$$\mathscr{H}(t) = \mathscr{H}_{\mathrm{S}}^{\circ} + \mathscr{H}_{\mathrm{E}}^{\circ} + \mathscr{H}_{\mathrm{SE}} + \mathscr{H}_{\mathrm{S}}(t) + \mathscr{H}_{\mathrm{E}}(t), \tag{1}$$

where $\mathscr{H}_{\mathrm{S}}^{\circ}$ is the time-independent Hamiltonian of the system, $\mathscr{H}_{\mathrm{E}}^{\circ}$ is the time-independent Hamiltonian of the local environment, $\mathscr{H}_{\mathrm{SE}}$ is the coupling between the system and the local environment with strength ω_{SE}, $\mathscr{H}_{\mathrm{S}}(t)$ is the external drive applied to the system with amplitude ω_1, and $\mathscr{H}_{\mathrm{E}}(t)$ denotes the fluctuations in the local environment. Since the fluctuations should not drive the lattice away from equilibrium, $\mathscr{H}_{\mathrm{E}}(t)$ is chosen to be diagonal in the eigenbasis $\{|\phi_j\rangle\}$ of $\mathscr{H}_{\mathrm{E}}^{\circ}$, represented by

$$\mathscr{H}_{\mathrm{E}}(t) = \sum_j f_j(t)|\phi_j\rangle\langle\phi_j|, \tag{2}$$

where $f_j(t)$ is assumed to be independent, Gaussian, δ-correlated stochastic variables with zero mean and standard deviation κ, i.e., $\overline{f_j(t)} = 0$ and $\overline{f_j(t_1)f_j(t_2)} = \kappa^2\delta(t_1 - t_2)$.

The Liouville–von Neumann equation for the single system and its environment is given by

$$\frac{d}{dt}\tilde{\rho}(t) = -i[H(t), \tilde{\rho}(t)], \tag{3}$$

where $\tilde{\rho}(t)$ denotes the density matrix of the system-environment pair in the interaction representation and $H(t)$ is the time-dependent part of the Hamiltonian expressed in the interaction representation. To express the solution of Eq. (3) for a finite time-interval from t to $t + \Delta t$ (used later as a course-graining interval) for the dynamics of the system part (denoted by S), we take the trace over the environment variables (denoted by $\mathrm{Tr_E}$) to obtain

$$\tilde{\rho}_{\mathrm{S}}(t + \Delta t) = \tilde{\rho}_{\mathrm{S}}(t) - i\int_t^{t+\Delta t} dt_1 \mathrm{Tr_E}[H_{\mathrm{eff}}(t_1), \tilde{\rho}(t_1)], \tag{4}$$

where $\tilde{\rho}_{\mathrm{S}}(t)$ denotes the system density matrix in the interaction representation $H_{\mathrm{eff}}(t) = H_{\mathrm{S}}(t) + H_{\mathrm{SE}}(t)$, with the Hamiltonians in the roman font denoting their forms in the interaction representation. The commutator involving $H_{\mathrm{E}}(t_1)$ vanishes due to the partial trace over the environment's degrees of freedom. On the right-hand side, the density matrix at time t_1 can be written as $\tilde{\rho}(t_1) = U(t_1, t)\tilde{\rho}(t)U^{\dagger}(t_1, t)$, where $U(t_1, t)$ denotes the propagator for the system and the environment pair from time t to t_1 in the Hilbert space. The trailing t in the propagator is omitted for notational simplicity in the rest of the paper. Starting from the Schrödinger equation, $U(t_1)$ can be expressed as

$$\begin{aligned} U(t_1) &= \mathbb{I} - i\int_t^{t_1} H(t_2)U(t_2)dt_2, \\ U(t_1) &= \mathbb{I} - i\int_t^{t_1} H_{\mathrm{eff}}(t_2)U(t_2)dt_2 - i\int_t^{t_1} H_{\mathrm{E}}(t_2)U(t_2)dt_2. \end{aligned} \tag{5}$$

It is assumed that $t_1 - t \ll \frac{1}{\omega_1}, \frac{1}{\omega_{\mathrm{SE}}}$ and the evolution due to H_{eff} during the interval from t to t_2 is negligible; the density matrix evolves from t to t_2 solely under H_{E} with a propagator denoted by $U_{\mathrm{E}}(t_2)$. With this approximation Eq. (5) can be written as

$$\begin{aligned} U(t_1) &\approx \mathbb{I} - i\int_t^{t_1} H_{\mathrm{eff}}(t_2)U_{\mathrm{E}}(t_2)dt_2 - i\int_t^{t_1} H_{\mathrm{E}}(t_2)U_{\mathrm{E}}(t_2)dt_2, \\ U(t_1) &\approx U_{\mathrm{E}}(t_1) - i\int_t^{t_1} H_{\mathrm{eff}}(t_2)U_{\mathrm{E}}(t_2)dt_2, \end{aligned} \tag{6}$$

where $U_{\mathrm{E}}(t_1) = \mathbb{I} - i\int_t^{t_1} H_{\mathrm{E}}(t_2)U_{\mathrm{E}}(t_2)dt_2$.

It is evident from the expression (6) that the propagator is finite in the instances of fluctuations (through the presence of U_{E}) and infinitesimal in H_{eff} (only a first-order appearance). Substituting Eq. (6) in Eq. (4), we get

$$\begin{aligned} &\tilde{\rho}_{\mathrm{S}}(t + \Delta t) \\ &= \tilde{\rho}_{\mathrm{S}}(t) - i\int_t^{t+\Delta t} dt_1 \mathrm{Tr_E}[H_{\mathrm{eff}}(t_1), U_L(t_1)\tilde{\rho}(t)U_L^{\dagger}(t_1)] \\ &\quad - \int_t^{t+\Delta t} dt_1 \int_t^{t_1} dt_2 \mathrm{Tr_E}[H_{\mathrm{eff}}(t_1), H_{\mathrm{eff}}(t_2)U_{\mathrm{E}}(t_2)\tilde{\rho}(t)U_{\mathrm{E}}^{\dagger}(t_1) \\ &\quad - U_{\mathrm{E}}(t_1)\tilde{\rho}(t)U_L^{\dagger}(t_2)H_{\mathrm{eff}}(t_2)] + O\big(H_{\mathrm{eff}}^3\big), \end{aligned} \tag{7}$$

where $O(H_{\mathrm{eff}}^3)$ indicates terms of the order of cubic or higher powers of H_{eff}, which we ignore. Next the Born approximation is used, i.e., at the beginning of the coarse-graining interval, the density matrix for the whole ensemble is factorized into that of the system and the environment, as

$$\rho(t) = \rho_S(t) \otimes \rho_{\mathrm{E}}^{\mathrm{eq}}, \tag{8}$$

where $\rho(t) = \overline{\tilde{\rho}(t)}$. The Born approximation and the assumption of the nature of the fluctuation provide the desired regulator in the second order under an ensemble average as

$$\overline{U_{\mathrm{E}}(t_1)\tilde{\rho}(t)U_{\mathrm{E}}^{\dagger}(t_2)} = \rho_{\mathrm{S}}(t) \otimes \rho_{\mathrm{E}}^{\mathrm{eq}} e^{-\kappa^2|t_1 - t_2|/2}. \tag{9}$$

Substituting Eq. (9) in Eq. (7) and performing the regular course-graining procedure [23], we obtain the FRQME given in the form

$$\frac{d}{dt}\rho_{\rm S}(t) = -i\,{\rm Tr}_{\rm E}\big[H_{\rm eff}(t),\rho_{\rm S}(t)\otimes\rho_{\rm E}^{\rm eq}\big]^{\rm sec} - \int_0^\infty d\tau\,{\rm Tr}_{\rm E}\big[H_{\rm eff}(t), \times\big[H_{\rm eff}(t-\tau),\rho_{\rm S}(t)\otimes\rho_{\rm E}^{\rm eq}\big]\big]^{\rm sec} e^{-|\tau|/\tau_c}, \quad (10)$$

where $\tau_c = 2/\kappa^2$ and the superscript sec stands for secular approximation that involves ignoring the fast oscillating terms in the quantum master equation. We note that since $H_{\rm eff}$ contains the drive term, the DID originates from the double commutator under the integral in Eq. (10). Equation (10) is in GKLS form, preserves the trace of the density matrix, and is completely positive. We note that the above master equation is derived under the assumption of a timescale separation which had been used while constructing the propagator. In terms of the variables used above, the timescale separation can be written as $\omega_1\tau_c \ll 1$ and $\omega_{\rm SE}\tau_c \ll 1$, i.e., the characteristic timescale of the decay of the autocorrelation of the fluctuations (τ_c) is assumed to be much shorter than the timescale over which the system evolves.

III. DRIVEN-DISSIPATIVE DYNAMICS OF A SINGLE QUBIT

To investigate the effect of DID on quantum gate operations, we apply the FRQME on a single-qubit system coupled to its local environment. As a particular physical realization of the qubit, we consider spin-1/2 systems having gyromagnetic ratio γ and placed in a static, homogeneous magnetic field $\mathbf{B}_\circ = B_\circ\hat{k}$ and an external resonant circularly polarized drive of the form $\mathbf{B}_1 = B_1[\cos(\omega t+\phi)\hat{i} + \sin(\omega t+\phi)\hat{j}]$ [where ω is the frequency of the drive, chosen to be equal to the Larmor frequency of the system ($\omega_\circ = -\gamma B_\circ$) and at time $t = 0$, and $\mathbf{B}_1$ makes an angle ϕ with respect to the x axis] is applied on the system. In the above, $\hat{i}$, $\hat{j}$, and $\hat{k}$ indicate the unit vectors in the x, y, and z directions, respectively, in a right-handed coordinate system.

The system-environment coupling can be modeled as a passive coupling described by a Jaynes-Cummings Hamiltonian of the form $\mathscr{H}_{\rm SE} = \omega_{\rm SE}(I_+L_- + I_-L_+)$, where I and L are the spin angular momentum operators of the system and the corresponding operators of the local environment, respectively, with $I_\pm = (I_x \pm iI_y)$ and similar definitions for the L counterparts. The choice of a Jaynes-Cummings Hamiltonian over a Caldeira-Leggett form is to account for both the longitudinal and the transverse relaxation appearing in the relaxation superoperator, as shown later [24,25]. We observe that ${\rm Tr}_{\rm E}\{L_\pm\rho_{\rm E}^{\rm eq}\} = 0$ leads to vanishing first-order contribution of $\mathscr{H}_{\rm SE}$ to system dynamics. On the other hand, ${\rm Tr}_{\rm E}\{L_\pm L_\mp\rho_{\rm E}^{\rm eq}\} = (1\pm m)/2$ leads to an equilibrium polarization of the system of m.

An application of the FRQME on this system results in the equation in the Liouville space

$$\frac{d\hat{\rho}_{\rm S}}{dt} = \hat{\hat{\Gamma}}\hat{\rho}_{\rm S} = \big[-i\hat{\hat{\mathcal{L}}}^{(1)}_{\rm drive} - \hat{\hat{\mathcal{L}}}^{(2)}_{\rm drive} - \hat{\hat{\mathcal{L}}}^{(2)}_{\rm system\text{-}env}\big]\hat{\rho}_{\rm S}, \quad (11)$$

where $-i\hat{\hat{\mathcal{L}}}^{(1)}_{\rm drive}$ is the Liouville superoperator or Liouvillian for the corresponding $-i[H_{\rm S},\rho_{\rm S}]$ term in the master equation. We assume that the system-environment coupling does not appear in the first order and no cross term between $H_{\rm S}$ and $H_{\rm SE}$ survives the ensemble average. In addition, $\hat{\hat{\mathcal{L}}}^{(2)}_{\rm drive}$ and $\hat{\hat{\mathcal{L}}}^{(2)}_{\rm system\text{-}env}$ are the second-order drive-induced decoherence and regular relaxation terms, respectively. With the explicit form of the complete superoperator, $\hat{\hat{\Gamma}}$ in Eq. (11) can be expressed as

$$\frac{d}{dt}\begin{pmatrix}\rho_{\rm S,11}\\ \rho_{\rm S,12}\\ \rho_{\rm S,21}\\ \rho_{\rm S,22}\end{pmatrix} = \begin{pmatrix} -\frac{\omega_1^2\tau_c}{2} - \frac{1-m}{2T_1} & \xi & \xi^\star & \frac{\omega_1^2\tau_c}{2} + \frac{1+m}{2T_1} \\ -\xi^\star & -\frac{\omega_1^2\tau_c}{2} - \frac{1}{T_2} & \eta^\star & \xi^\star \\ -\xi & \eta & -\frac{\omega_1^2\tau_c}{2} - \frac{1}{T_2} & \xi \\ \frac{\omega_1^2\tau_c}{2} + \frac{1-m}{2T_1} & -\xi & -\xi^\star & -\frac{\omega_1^2\tau_c}{2} - \frac{1+m}{2T_1} \end{pmatrix}\begin{pmatrix}\rho_{\rm S,11}\\ \rho_{\rm S,12}\\ \rho_{\rm S,21}\\ \rho_{\rm S,22}\end{pmatrix}. \quad (12)$$

This dynamical equation contains three types of terms, viz., (i) the first-order nutation terms, given by $\xi = ie^{i\phi}\omega_1/2$, where $\omega_1 = -\gamma B_1$ is the drive amplitude in the angular frequency units (the axis of the drive may be chosen by suitably adjusting ϕ); (ii) the second-order DID terms on the diagonal and on the antidiagonal, given by $\omega_1^2\tau_c$ and $\eta = e^{2i\phi}\omega_1^2\tau_c/2$, respectively; and (iii) the second-order relaxation terms, which include T_1 and T_2 to denote longitudinal and transverse relaxation times, respectively [16]. The longitudinal and the transverse relaxation times (T_1 and T_2, respectively) are defined to be the characteristic times with which the expectation values of I_z and $I_\pm$ relax back to their respective equilibrium values. We note that the cross terms between $\mathscr{H}_{\rm S}$ and $\mathscr{H}_{\rm SE}$ vanish since ${\rm Tr}_{\rm E}\{\mathscr{H}_{\rm SE}\rho_{\rm E}^{\rm eq}\} = 0$. In the interaction picture, $\mathscr{H}_{\rm SE}$ leads to the Lorentzian forms of the spectral densities in the expressions of the relaxation rates with a strength of $\omega_{\rm SE}^2\tau_c$ due to the presence of the regulator $\exp(-|\tau|/\tau_c)$. We estimate T_1 and T_2 as proportional to $\omega_{\rm SE}^2\tau_c$ using this model to obtain the dependence of the relaxation terms on the regulator which appears from the fluctuations in the environment. The assumption is amply justified if the only energy levels of the environment contribute significantly to the system dynamics whose energy separation ($\omega_{\rm E}$ in angular frequency units) matches the energy spacing of the system, in which case the Lorentzian factor $1/(1+\omega_{\circ{\rm E}}^2\tau_c^2)$, with $\omega_{\circ{\rm E}} = \omega_\circ - \omega_{\rm E}$ and $\omega_\circ \sim \omega_{\rm E}$, reduces to 1.

In the above, the drive was applied on resonance with the spin Larmor frequency. If the drive is applied with a resonance offset $\Delta\omega$, then the strengths of the real and imaginary parts of the second-order contribution of the drive in a rotating frame of $\omega_\circ + \Delta\omega$ are given by $-\omega_1^2\tau_c/C$ and $\omega_1^2\Delta\omega\tau_c^2/C$, respectively, where $C = 1 + \Delta\omega^2\tau_c^2$. The imaginary component indicates the dynamic Stark shift or the light shift and the real part is the DID. As such, the drive-induced dissipation and the light shifts are nothing but a Kramers-Kronig pair. The expression of the dynamic Stark shift reduces to the familiar form of $\omega_1^2/\Delta\omega$ when $\Delta\omega\tau_c \gg 1$. We note that the DID being the Kramers-Kronig pair of the light shift is different from the previously known forms of drive-dependent dissipation and had been discussed in detail in the work of Chakrabarti and Bhattacharyya [16].

To validate the FRQME, we use Eq. (12) to analyze a three-pulse block $R_3 = \{\pi, -2\pi, \pi\}$, previously described in Chakrabarti and Bhattacharyya's work [17]. A straightforward analysis assuming $\omega_1 \gg \frac{1}{T_1}, \frac{1}{T_2}$, which holds for the aforementioned experiment, shows that after application of the pulse block, the magnetization, which is proportional to $\mathrm{Tr}\{\sigma_z\rho_S\}$, is reduced by a factor of $e^{-(R_{\mathrm{eff}}+\omega_1^2\tau_c)T}$, where T is the duration of the three-pulse block and R_{eff} denotes $\frac{1}{T_1} + \frac{1}{T_2}$. We will use the above assumption in the subsequent calculations as well, since this does not impose an upper bound on the drive amplitude. In order to arrive at this factor, Eq. (12) has been consecutively solved for three successive pulses and finally the z component of magnetization has been computed. This expression exactly describes the behavior of the nutating magnetization of the aforementioned three-pulse block [17].

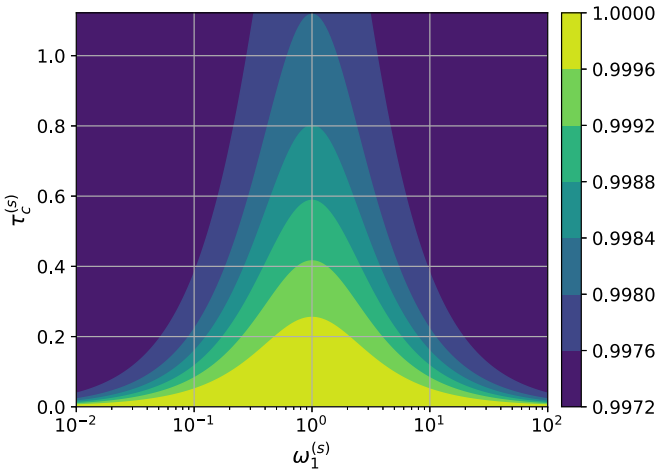

FIG. 1. Filled contours showing the fidelity as a function of $\omega_1^{(s)}$ and $\tau_c^{(s)}$. We note that the maximum value of the fidelity does not depend on m; for $\tau_c^{(s)} \to 0$, we obtain the maximum fidelity to be 1 for all values of m. In this plot, m has been chosen as 0.1 (which appears only in the initial density matrix). The central vertical grid at $\omega_1^{(s)} = 1$ shows the position of the optimum drive amplitude. For a particular value of $\omega_1^{(s)}$, the value of fidelity increases with the lowering of $\tau_c^{(s)}$. We note that $\tau_c^{(s)} \to 0$ corresponds to the complete absence of all second-order terms, in which case the evolution of the qubit is unitary. Under this condition, the fidelity is 1 for all values of ω_1 as shown by the yellow (light gray) region at the bottom of the plot. The range of values for which a single color has been used in the plot is shown in the colorbar on the right with the upper and lower bounds of the range.

IV. FIDELITY OF THE HADAMARD GATE

A. Analytical approach

We consider the situation of a single Hadamard gate applied on a mixed state written in a pseudopure form $\rho_0 = \frac{(1-m)}{2}\mathbb{I} + m|0\rangle\langle 0|$. A Hadamard gate is realized by the unitary propagator $U_{\mathrm{Hadamard}} = e^{iI_y(\pi/2)}e^{-iI_x\pi}$ [26]. The practical realization of this gate on a single spin qubit will require two square pulses to be applied about the x axis and $-y$ axis for durations π/ω_1 and $\pi/2\omega_1$, respectively. If the system evolves without any dissipation during the application of the gate, the final density matrix would be $\rho = \frac{1}{2}(\mathbb{I} + m\sigma_x)$.

On the other hand, if we consider the dissipative evolution of the system (from the initial ρ_0) as dictated by Eq. (12), we obtain a mixed-state density matrix $\rho' = \frac{1}{2}(\mathbb{I} + ma\,\sigma_x)$ at the end of the gate operation, where $a = \exp[-\frac{3\pi}{2}(\frac{R_{\mathrm{eff}}}{\omega_1} + \omega_1\tau_c)]$. To estimate the departure from the unitary behavior, we calculate the fidelity using the definition [27,28]

$$F(\rho, \rho') = \left(\mathrm{Tr}\sqrt{\sqrt{\rho}\rho'\sqrt{\rho}}\right)^2. \tag{13}$$

The fidelity between the expected density matrix ρ and the obtained density matrix ρ', for this particular case, turns out to be

$$F = \tfrac{1}{2}[(1 + m^2a) + \sqrt{(1-m^2)(1-m^2a^2)}]. \tag{14}$$

The above form of fidelity has a maximum value for an optimum value of the drive amplitude ω_1^{opt}, given by

$$\omega_1^{\mathrm{opt}} = \sqrt{R_{\mathrm{eff}}/\tau_c} \approx \omega_{\mathrm{SE}}, \tag{15}$$

where, to obtain the expression (15), a simplifying form $R_{\mathrm{eff}} = \frac{1}{T_1} + \frac{1}{T_2} \sim \omega_{\mathrm{SE}}^2\tau_c$ is assumed.

To show the dependence of the fidelity on the drive amplitude ω_1 in units of ω_{SE}, we rewrite the expression for a as $a = \exp\{-\frac{3\pi}{2}\tau_c^{(s)}(\omega_1^{(s)} + 1/\omega_1^{(s)})\}$, where $\tau_c^{(s)} = \omega_{\mathrm{SE}}\tau_c$ denotes a scaled value of τ_c and $\omega_1^{(s)} = \omega_1/\omega_{\mathrm{SE}}$ denotes a scaled value of ω_1. In Fig. 1 the filled contours depict the fidelity of the Hadamard gate from Eq. (14) for various combinations of $\tau_c^{(s)}$ and $\omega_1^{(s)}$. For a given $\tau_c^{(s)}$ the maximum fidelity is achieved for $\omega_1^{(s)} = 1$, i.e., for $\omega_1 = \omega_{\mathrm{SE}}$. It is also evident that for smaller $\tau_c^{(s)}$, the fidelity attains a higher value with a wider range of the drive amplitude. Therefore, the fidelity attains a maximum value when the drive amplitude ω_1 is of the order of the system-environment coupling ω_{SE}.

B. Numerical approach

In the previous treatment, we obtained a simplified expression for the fidelity of the Hadamard gate under a few simplifying assumptions. In this section, we numerically solve Eq. (12) for the two pulses of the Hadamard gate without the aforementioned assumptions.

The fidelity has been calculated numerically using Eq. (13) and plotted as a function of the scaled variables $\tau_c^{(s)}$ and $\omega_1^{(s)}$

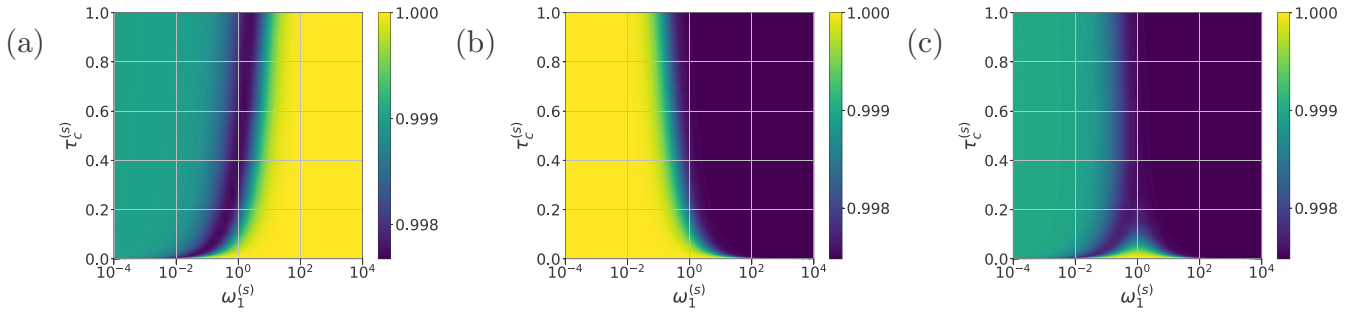

FIG. 2. Filled contour plots of fidelity numerically calculated by solving Eq. (12) for the Hadamard gate. The initial density matrix has been chosen to be the same as for the analytical case. In all three plots, the first-order contributions of the drive is retained. (a) Fidelity with only the relaxation term in the second order [$\hat{\hat{\mathcal{L}}}^{(2)}_{\text{system-env}}$ of Eq. (11)]. The plot shows higher fidelity with a large drive amplitude (large $\omega_1^{(s)}$). For large $\omega_1^{(s)}$, the gate time is short and hence the relaxation acts for a shorter duration. As a result, the fidelity is higher for larger $\omega_1^{(s)}$. (b) Fidelity with only the drive term in the second order [$\hat{\hat{\mathcal{L}}}^{(2)}_{\text{drive}}$ of Eq. (11)]. Here the larger $\omega_1^{(s)}$ results in a strong DID effect and the fidelity decreases. (c) Effects of both terms. The competition between the two effects results in a peaked behavior for $\omega_1^{(s)}$.

in Fig. 2. Equation (12) has been solved numerically with $\omega_{\text{SE}} = 2\pi \times 10^2$ krad/s and $m = 0.1$. To analyze the behavior of the fidelity, we first plot the fidelity by considering only the relaxation due to system-environment coupling, but no drive-induced decoherence (as in a standard quantum master equation). We observe that, in general, the fidelity increases as we increase $\omega_1^{(s)}$, since for larger $\omega_1^{(s)}$ the gate operation time is shorter and as a result, the effect of the relaxation is smaller. For the low-$\tau_c^{(s)}$ regime the fidelity reaches the highest value for smaller-$\omega_1^{(s)}$ values compared to that of the high-$\tau_c^{(s)}$ regime. Next we plot fidelity keeping only the DID, but no relaxation terms, and find that the fidelity decreases when we increase $\omega_1^{(s)}$. In this case, for the low-$\tau_c^{(s)}$ regime the fidelity remains nearly 1 for higher-$\omega_1^{(s)}$ values compared to that of the high-$\tau_c^{(s)}$ regime. Their combined effects are reflected in Fig. 2(c) and optimality exists for a certain value of $\omega_1^{(s)} = 1$. This behavior corroborates the analytical expression of fidelity as given in Eq. (14).

V. MEASURE OF NONUNITARITY

In the previous sections, for the calculation of fidelity, we have used the form of the density matrix which contains the equilibrium polarization m and has a trace equal to 1. However, the effect of the equilibrium polarization in the $\hat{\hat{\Gamma}}$ matrix in the Liouville space is minuscule under the assumption of $\omega_1 \gg 1/T_1, 1/T_2$, which is an experimental reality in optical or magnetic resonance excitation schemes. As such, to rid ourselves of the necessity of using a suitable density matrix for the calculation of the efficacy of gates under DID and relaxation, we define a new quantity as a measure of nonunitarity and call it efficiency, $E = \text{Tr}(\mathscr{U}\mathscr{U}^\dagger)/(2^n)^2$, where $\mathscr{U} = e^{\hat{\hat{\Gamma}}T}$ is the propagator in Liouville space, with $\hat{\hat{\Gamma}}$ given in Eq. (11) and T the duration of the operation, and n is the number of qubits. The motivation behind introducing such a new quantity is that it does not depend on the choice of the initial state; it only produces the amount of nonunitarity emerging from the presence of system-environment coupling and drive during the implementation of the gate. For the calculation of the efficiency for a multistep sequence, the propagator has been constructed from the time-ordered products of the propagator of individual operations. Using the same protocol of calculating fidelity numerically, we generate $\mathscr{U}$ and plot the efficiency for the Hadamard gate and other multiqubit gates in logarithmic scale.

A. Single-qubit gate: Hadamard gate

We have made another attempt to study the nonunitary behavior of a two-level system (TLS) under the operation of the Hadamard gate by finding its efficiency. The plots are shown in Fig. 3. In the first plot, i.e., including only the relaxation terms and no DID, for a given efficiency E, $\tau_c^{(s)}$ is proportional to $\omega_1^{(s)}$ with both of the axes being in logarithmic scale, since $E \sim \frac{1}{4} + \frac{3}{4}e^{-3\pi\tau_c^{(s)}/\omega_1^{(s)}}$. Thus we expect a linear contour with a positive slope as shown in Fig. 3(a). On the other hand, when only the DID is considered but no relaxation terms, then $\tau_c^{(s)}$ is inversely proportional to $\omega_1^{(s)}$, since $E \sim \frac{1}{4}(1 + e^{-\pi\tau_c^{(s)}\omega_1^{(s)}} + e^{-2\pi\tau_c^{(s)}\omega_1^{(s)}} + e^{-3\pi\tau_c^{(s)}\omega_1^{(s)}})$. Hence, we expect a linear contour with negative slope when both of the axes are in logarithmic scale as shown in Fig. 3(b). When their total effect is considered, the nature of the efficiency plot in Fig. 3(c) shows triangular behavior; fixed efficiency contours linearly increase with increasing $\omega_1^{(s)}$, reach a maximum at $\omega_1^{(s)} = 1$, and then decrease linearly.

B. Two-qubit gate: Controlled-NOT gate

As an example of a two-qubit gate, we investigate the controlled-NOT (CNOT) gate, which can be realized by the propagator [29]

$$U_{\text{CNOT}} = e^{-iI_y^{(2)}(\pi/2)} e^{-i(I_z^{(1)}+I_z^{(2)})(\pi/2)} e^{iI_z^{(1)}I_z^{(2)}\pi} e^{iI_y^{(2)}(\pi/2)}, \quad (16)$$

where the superscripts on the spin operators indicate the number of qubits on which the operators act. The qubit Larmor frequencies are assumed to have a small dispersion which does not have a noticeable impact on the relaxation terms. The implementation of the second operation of the sequence (from right to left) requires a scalar coupling between the qubits of the form $\mathscr{H}_J = 2\pi J I_z^{(1)} I_z^{(2)}$ and which acts with a duration $1/2J$. Figures 4(a) and 4(b) show the calculated efficiencies for the above sequence for $J = 10$ and 100 kHz, respectively, using only the relaxation terms in the second order. Since the

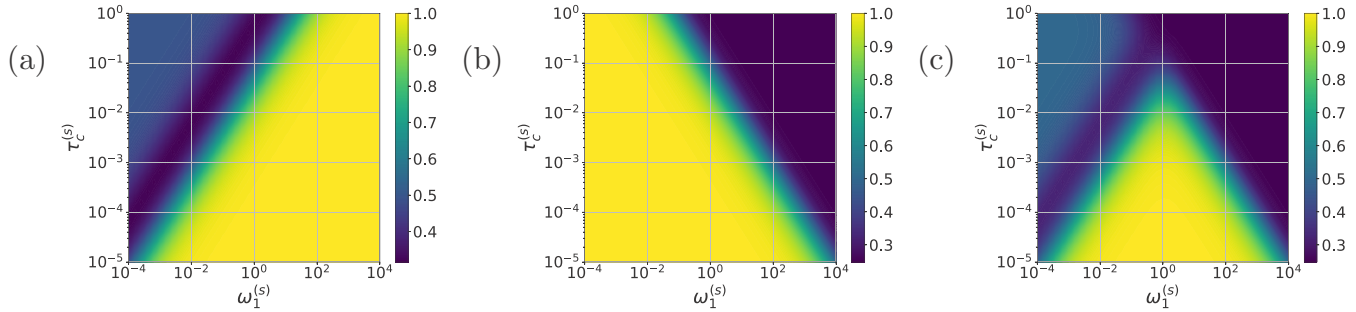

FIG. 3. Filled contour plots of efficiency E numerically calculated by solving Eq. (12) for the Hadamard gate. The $\hat{\bar{\Gamma}}_k$ matrix for the kth pulse has been calculated using the values mentioned in the text and the propagator $\mathscr{U}_k$ has been calculated using $\mathscr{U}_k = \exp(\hat{\bar{\Gamma}}_k \tau_k)$, where τ_k is the duration of the kth pulse. The time-ordered product of $\mathscr{U}_k$s provides the total propagator $\mathscr{U}$, which is used for the calculation of efficiency as defined in the text. In all three plots, the first-order contributions of the drive is retained. (a) Efficiency with only the relaxation term in the second order [$\hat{\bar{\mathcal{L}}}^{(2)}_{\text{system-env}}$ of Eq. (11)]. The plot shows higher efficiency with a large drive amplitude (large $\omega_1^{(s)}$) as in Fig. 2(a). (b) Efficiency with only the drive term in the second order [$\hat{\bar{\mathcal{L}}}^{(2)}_{\text{drive}}$ of Eq. (11)]. Here the larger $\omega_1^{(s)}$ results in a strong DID effect and the efficiency decreases linearly in logarithmic scale. (c) Effects of both terms. The competition between the two effects results in a triangular regime for the highest efficiency.

duration $1/2J$ is longer in the first case, the relaxation acts for a longer duration and hence the efficiency is lower for longer $\tau_c^{(s)}$ compared to that of the second case with $J = 100$ kHz. Hence, the efficiency drastically falls above $\tau_c^{(s)} = 10^{-2}$ for $J = 10$ kHz, shown in Fig. 4(a), in which the decay due to the relaxation is noticeably stronger. Figure 4(c) shows the contours of the efficiency with only the DID terms and no relaxation. The behavior is similar to the Hadamard case since the drive-induced decoherence behaves in an identical manner. Figures 4(d) and 4(e) show the filled contours of the efficiencies including both the DID and the relaxation terms for $J = 10$ and 100 kHz, respectively. The first case clearly inherits the less efficient regime from the relaxation effects during the longer gate operation time.

C. Three-qubit gate: Toffoli gate

We have done the same treatment for a three-qubit gate, the Toffoli gate. The propagator required to implement the Toffoli

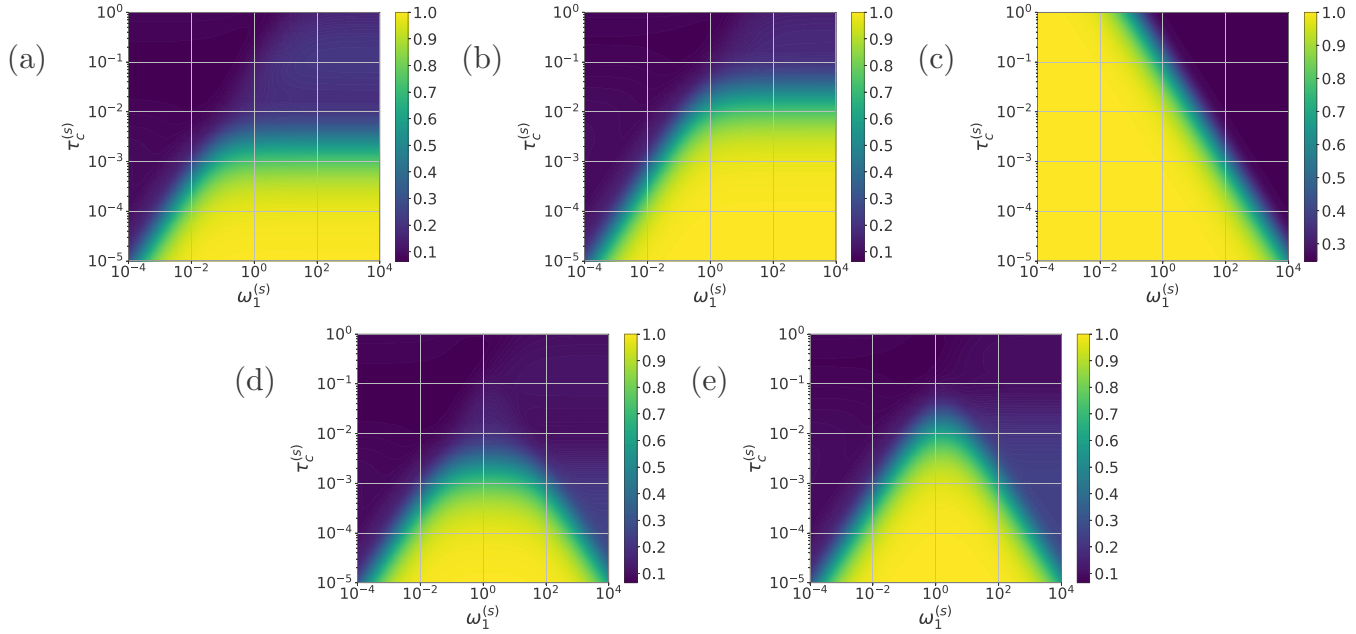

FIG. 4. Filled contours for the efficiency of the CNOT gate as realized by the pulse sequence given by Eq. (16). In all plots the first-order contribution of the drive is retained. The efficiency with only the relaxation term in the second order [$\hat{\bar{\mathcal{L}}}^{(2)}_{\text{system-env}}$ of Eq. (11)] is shown for (a) $\omega_J = 10$ kHz and (b) $\omega_J = 100$ kHz. The plot shows higher efficiency with a large drive amplitude (large $\omega_1^{(s)}$) as in Fig. 3(a). For a larger value of ω_J [in (b)] the gate duration is shorter; this results in higher efficiency since the relaxation acts for less time. (c) Efficiency with only the drive term in the second order [$\hat{\bar{\mathcal{L}}}^{(2)}_{\text{drive}}$ of Eq. (11)]. Here the larger $\omega_1^{(s)}$ results in a strong DID effect and the efficiency decreases linearly in logarithmic scale as in the case of the Hadamard gate [shown in Fig. 3(b)]. Effects of both terms for (d) $\omega_J = 10$ kHz and (e) $\omega_J = 100$ kHz. The competition between the two effects results in a triangular regime for the highest efficiency.

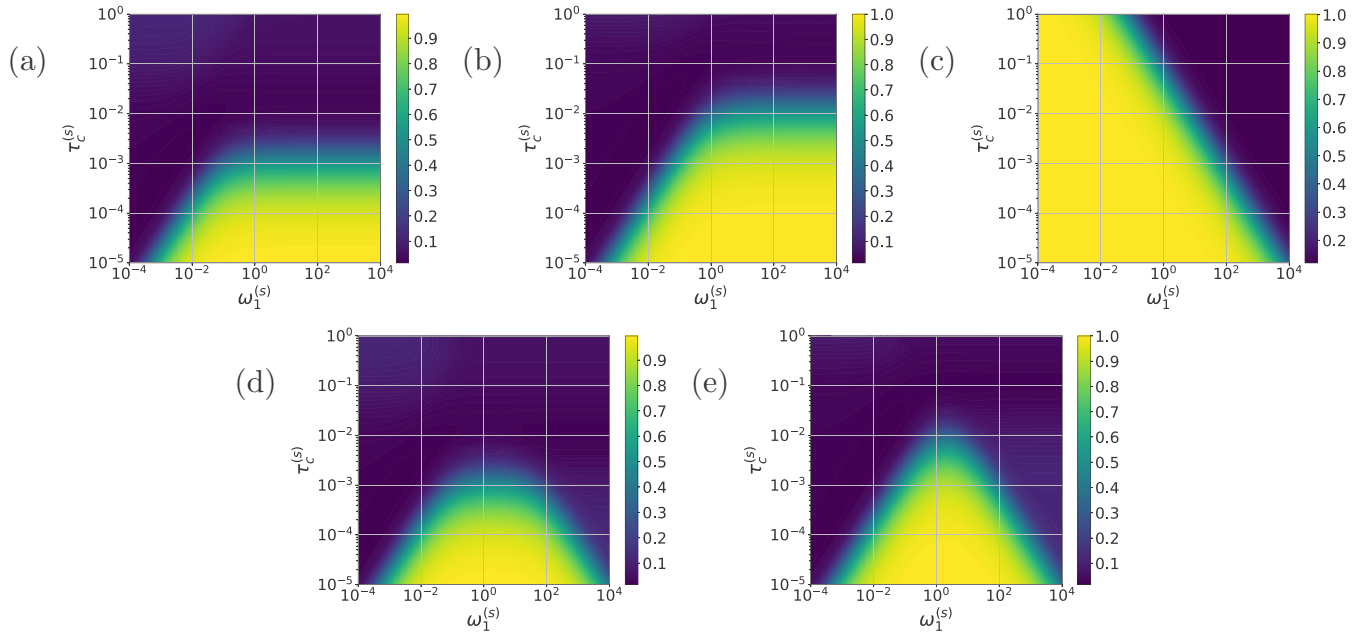

FIG. 5. Filled contours for the efficiency of the Toffoli gate as given in Eq. (18). In all plots the first-order contribution of the drive is retained. The efficiency with only the relaxation term in the second order [$\hat{\tilde{\mathcal{L}}}^{(2)}_{\text{system-env}}$ of Eq. (11)] is shown for (a) $\omega_J = 10$ kHz and (b) $\omega_J = 100$ kHz. The plot shows higher efficiency with a large drive amplitude (large $\omega_1^{(s)}$) as in Fig. 3(a). For a larger value of ω_J [in (b)] the gate duration is shorter; this results in higher efficiency since the relaxation acts for less time. (c) Efficiency with only the drive term in the second order [$\hat{\tilde{\mathcal{L}}}^{(2)}_{\text{drive}}$ of Eq. (11)]. Here the larger $\omega_1^{(s)}$ results in a strong DID effect and the efficiency decreases linearly in logarithmic scale as in the case of the Hadamard gate [shown in Fig. 3(b)]. Effects of both terms for (d) $\omega_J = 10$ kHz and (e) $\omega_J = 100$ kHz. The competition between the two effects results in a triangular regime for the highest efficiency.

gate is [30]

$$\begin{aligned} U_{\text{Toffoli}} = {} & e^{iI_x^{(3)}(\pi/2)} e^{-i(I_z^{(1)}I_z^{(2)}+I_z^{(2)}I_z^{(3)}+I_z^{(3)}I_z^{(1)})(\pi/2)} \\ & \times e^{iI_x^{(3)}(\pi/2)} e^{-i(I_z^{(1)}I_z^{(2)}+I_z^{(2)}I_z^{(3)}+I_z^{(3)}I_z^{(1)})(\pi/2)} \\ & \times e^{-iI_y^{(3)}(\pi/2)} e^{-i(I_z^{(1)}I_z^{(2)}+I_z^{(2)}I_z^{(3)}+I_z^{(3)}I_z^{(1)})(\pi/2)} e^{-iI_y^{(3)}(\pi/2)}. \end{aligned} \tag{17}$$

The second, fourth, and sixth operations are the evolutions under scalar coupling Hamiltonians given by

$$\begin{aligned} & \mathscr{H}_{\text{J}}^{(12)} + \mathscr{H}_{\text{J}}^{(23)} + \mathscr{H}_{\text{J}}^{(13)} \\ & \quad = 2\pi \left(J_{12} I_z^{(1)} I_z^{(2)} + J_{23} I_z^{(2)} I_z^{(3)} + J_{13} I_z^{(1)} I_z^{(3)} \right). \end{aligned} \tag{18}$$

The duration of the operations under these couplings is effectively $1/4J$, where J is the smallest of the three coupling constants. Figures 5(a) and 5(b) show the contours of the efficiency when only the relaxation terms are taken into account, for $J = 10$ and 100 kHz, respectively. For smaller J, the duration of the gate is longer and hence the effect of the relaxation is stronger, resulting in reduced efficiency of the gate. The reduced efficiency is indicated by the smaller region of $E \sim 1$ in Fig. 5(a) compared to that in Fig. 5(b). When only the DID terms are taken into account, but not the relaxation, the resulting behavior [as shown in Fig. 5(c)] is similar to the case of a single pulse. The total effects of the DID and the relaxation terms for $J = 10$ and 100 kHz are shown in Figs. 5(d) and 5(e), respectively, which are similar to the final figures of the CNOT gate [Figs. 4(d) and 4(e)].

VI. DISCUSSION

The speed of a classical computer is specified in terms of its clock speed. Similarly, for a quantum computer, the period of Rabi oscillation or nutation defines the time required for a quantum gate operation. As such, the frequency of Rabi oscillation (ω_1 in our work) is effectively the clock speed. Thus our result indicates that maximum fidelity can be achieved only for a specific clock speed, which is referred to as the optimal clock speed of the quantum gates. The optimum value of the drive amplitude has been shown to be identical for single- and multiple-qubit gates. The precise form of the optimum drive amplitude would also depend on the drive-independent operations used in the gate operation. For example, in the case of CNOT and Toffoli gates, the relaxation during the evolution under the qubit-qubit couplings results in a flatter optimality condition in particular with a weaker-coupling value (smaller value of J). In such cases, we find (numerically) a flatter optimality condition for the drive.

While this work specifically uses the FRQME, other known forms of drive-dependent decay terms, such as the fourth-order photon-phonon dissipative terms (second order in the drive and second order in qubit-environment coupling) as given by Müller and Stace using the Keldysh formalism, can also be incorporated in this analysis [31,32]. This fourth-order drive-coupling cross term has the form $\omega_1^2 \tilde{T}$, where $\tilde{T}$ is a function of the qubit-environment coupling and other relevant frequencies. We note that the origin and the nature of DID are different from the aforementioned fourth-order term since DID does not explicitly contain the system-environment

coupling. As such, all conclusions drawn above remain valid, although the form of the optimum value of ω_1 would change.

An external drive on a TLS gives rise to Rabi oscillation in the first order. In the second order, two instances of the drive act, at times t_1 and t_2 (with $t_1 > t_2$), with the instances being a secular pair. For example, suppose that I_+ $(=I_x + iI_y)$ acts at time t_1 with phase $\exp(i\Delta\omega t_1)$, where $\Delta\omega = \omega - \omega_\circ$ (=0 if the drive is resonant), and its secular pair I_- $(=I_x - iI_y)$ acts at time t_2 with phase $\exp(-i\Delta\omega t_2)$. This mimics a flip-flop transition for the system. Between t_1 and t_2, the environment evolves under fluctuation and dephases. Ensemble averaging on the dephasing provides a decay. The mechanism is not similar to previously known forms of drive-induced dissipation. Our original work on the fluctuation-regulated quantum master equation discussed this issue extensively [16]. Our formalism predicts that the overall contribution should be in the form of a complex susceptibility, where the real absorptive part provides a decay and the imaginary dispersive part provides the shift [16]. The light shift or the Bloch-Siegert shifts (which are a Kramers-Kronig pair of the DID) are physically explained as an effective field which adds to the Zeeman direction to cause a shift in the resonance frequency. On the other hand, DID is an additional contribution to the lifetime of the levels of the TLS under consideration.

Earlier, Plenio and Knight obtained an optimal range of the drive power of laser-driven trapped-ion systems using the following arguments [33]. On such systems, a lower drive power results in a longer computation time during which the system may undergo a spontaneous emission. On the other hand, a too high laser power leads to ionization. As such, one obtains a small window of laser power for practical operating considerations of quantum information processing on such systems. Later they showed that even for a laser power which was not strong enough to cause ionization, there might be leakages to other atomic levels because of the laser field (off-resonance) acting between the original and the leak level [34]. They found that such leakages did not have any dependence on the laser power. We note that their analysis is confined to multilevel trapped-ion systems and any mechanism similar to DID is not taken into account. On the contrary, we consider two-level systems without any leakage (no additional levels) and show that DID and qubit-environment coupling can lead to an optimality condition.

To implement the gate operation, one may also use a shaped pulse for which the amplitude, frequency, and phase may be a function of time. Usually these variations are much slower compared to the timescale of the fluctuations. We outline here two approaches to deal with the shaped pulses. In the first approach, a shaped pulse can be constructed as a sequence of narrow square pulses of fixed parameters. For each of these pulses, one can construct a suitable superoperator $\hat{\hat{\Gamma}}$. Sequential application of respective $\hat{\hat{\Gamma}}$'s will lead to the final density matrix. This approach is particularly suitable for numerical evaluation of the propagator. In the second approach, which is more suitable for analytical evaluation of the propagator, $\hat{\hat{\Gamma}}$ in Eq. (11) can simply be expressed as a function of time since H_S has time-dependent parameters. In such cases, the finite-time propagator is given by $\mathcal{T}\exp[\int_{t_i}^{t_f} dt' \hat{\hat{\Gamma}}(t')]$, where t_i and t_f indicate the time instances of the beginning and the end of the shaped pulse, respectively, and $\mathcal{T}$ is the Dyson time-ordering operator.

It is evident that the clock speed of the highest-fidelity single-qubit and multiqubit operations has an optimum value. For multiqubit systems, one encounters one more complexity, which we discuss here. It is known that the time required for an arbitrary transitional-selective pulse, and hence the overall operation time of a specific task in quantum computation on a multiqubit network, is limited by the strength of the qubit-qubit coupling (J) [35]. To be adequately selective, a square pulse must have a duration τ_p which is inversely proportional to J, i.e., $\tau_p \gtrsim \frac{1}{J}$. This in turn indicates that the drive amplitude ω_1 must be less than or of the order of J (keeping the flip angle constant). Therefore, to achieve maximum fidelity on such a multiqubit system, one must satisfy the condition $\omega_1^{\rm opt} \sim \omega_{\rm SE} \leqslant J$. Such a restriction may not be achievable for an architecture based on nuclear spins, but may be engineered in quantum dots or superconducting flux qubits.

VII. CONCLUSION

We have shown that the speeding up of gate operations on single or multiple qubits by increasing the drive amplitude may have detrimental effects on the fidelity or the efficiency of the desired operation. There are two competing processes which affect the fidelity, viz., relaxation from the qubit-environment coupling and the DID. For a drive amplitude much lower than the optimum value, the relaxation terms dominate and the increase in the amplitude of the drive (ω_1) results in faster gate operation with higher fidelity. In contrast, for a drive amplitude greater than the optimum value, the DID processes dominate and reduce the fidelity. Therefore, an optimum value for ω_1 exists for which the fidelity of a quantum operation reaches its maximum. The optimum value of the drive amplitude is proportional to the strength of the qubit-environment coupling. Consequently, faster gate operations with maximum fidelity would be aided by better isolation of the qubit network from the environmental influences, as one expects intuitively. Finally, we conclude that the competition between the speed of a quantum gate and its fidelity is an intrinsic feature for open quantum systems. We envisage that the notion of drive-induced decoherence would play an important role in realistic implementation of fast and high-fidelity quantum gates.

ACKNOWLEDGMENTS

The authors wish to acknowledge Martin B. Plenio, Anil Kumar, Siddhartha Lal, and N. S. Vidhyadhiraja for helpful comments and discussions.

[1] D. Deutsch and R. Jozsa, Proc.: Math. Phys. Sci. **439**, 553 (1992).

[2] P. W. Shor, in *Proceedings 35th Annual Symposium on Foundations of Computer Science* (IEEE, Piscataway, 1994), pp. 124–134.

[3] L. K. Grover, Phys. Rev. Lett. **79**, 325 (1997).

[4] P. W. Shor, SIAM Rev. **41**, 303 (1999).

[5] N. A. Gershenfeld and I. L. Chuang, Science **275**, 350 (1997).

[6] J. I. Cirac and P. Zoller, Phys. Rev. Lett. **74**, 4091 (1995).

[7] D. G. Cory, A. F. Fahmy, and T. F. Havel, Proc. Natl. Acad. Sci. USA **94**, 1634 (1997).

[8] D. Loss and D. P. DiVincenzo, Phys. Rev. A **57**, 120 (1998).

[9] C. A. Ryan, O. Moussa, J. Baugh, and R. Laflamme, Phys. Rev. Lett. **100**, 140501 (2008).

[10] J. Bylander, S. Gustavsson, F. Yan, F. Yoshihara, K. Harrabi, G. Fitch, D. G. Cory, Y. Nakamura, J.-S. Tsai, and W. D. Oliver, Nat. Phys. **7**, 565 (2011).

[11] J. Yoneda, K. Takeda, T. Otsuka, T. Nakajima, M. R. Delbecq, G. Allison, T. Honda, T. Kodera, S. Oda, Y. Hoshi *et al.*, Nat. Nanotechnol. **13**, 102 (2018).

[12] W. Huang, C. H. Yang, K. W. Chan, T. Tanttu, B. Hensen, R. C. C. Leon, M. A. Fogarty, J. C. C. Hwang, F. E. Hudson, K. M. Itoh *et al.*, Nature (London) **569**, 532 (2019).

[13] D. P. DiVincenzo, Fortschr. Phys. **48**, 771 (2000).

[14] C. J. Ballance, T. P. Harty, N. M. Linke, M. A. Sepiol, and D. M. Lucas, Phys. Rev. Lett. **117**, 060504 (2016).

[15] C. Song, K. Xu, W. Liu, C.-P. Yang, S.-B. Zheng, H. Deng, Q. Xie, K. Huang, Q. Guo, L. Zhang *et al.*, Phys. Rev. Lett. **119**, 180511 (2017).

[16] A. Chakrabarti and R. Bhattacharyya, Phys. Rev. A **97**, 063837 (2018).

[17] A. Chakrabarti and R. Bhattacharyya, Europhys. Lett. **121**, 57002 (2018).

[18] S. Bertaina, S. Gambarelli, A. Tkachuk, I. N. Kurkin, B. Malkin, A. Stepanov, and B. Barbara, Nat. Nanotechnol. **2**, 39 (2007).

[19] R. G. DeVoe and R. G. Brewer, Phys. Rev. Lett. **50**, 1269 (1983).

[20] R. Boscaino and V. M. La Bella, Phys. Rev. A **41**, 5171 (1990).

[21] R. Boscaino, F. M. Gelardi, and J. P. Korb, Phys. Rev. B **48**, 7077 (1993).

[22] S. Nellutla, K.-Y. Choi, M. Pati, J. van Tol, I. Chiorescu, and N. S. Dalal, Phys. Rev. Lett. **99**, 137601 (2007).

[23] C. Cohen-Tannoudji, J. Dupont-Roc, and G. Gilbert, *Atom-Photon Interactions: Basic Processes and Applications* (Wiley-VCH, Weinheim, 2004).

[24] E. T. Jaynes, and F. W. Cummings, Proc. IEEE **51**, 89 (1963).

[25] A. O. Caldeira and A. J. Leggett, Phys. Rev. Lett. **46**, 211 (1981).

[26] R. Das, T. S. Mahesh, and A. Kumar, Chem. Phys. Lett. **369**, 8 (2003).

[27] A. Uhlmann, Rep. Math. Phys. **9**, 273 (1976)

[28] R. Jozsa, J. Mod. Opt. **41**, 2315 (1994).

[29] N. Linden, E. Kupce, and R. Freeman, Chem. Phys. Lett. **311**, 321 (1999).

[30] D. G. Cory, M. D. Price, and T. F. Havel, Physica D **120**, 82 (1998).

[31] L. V. Keldysh, Sov. Phys. JETP **20**, 1018 (1965).

[32] C. Müller and T. M. Stace, Phys. Rev. A **95**, 013847 (2017).

[33] M. B. Plenio and P. L. Knight, Phys. Rev. A **53**, 2986 (1996).

[34] M. B. Plenio and P. L. Knight, Proc. R. Soc. A **453**, 2017 (1997).

[35] M. Steffen, M. K. Lieven, Vandersypen, and I. L. Chuang, IEEE Micro **21**, 24 (2001).